Journal of Medical Radiation Sciences

Open Access

ORIGINAL ARTICLE

Reduction of metal artefacts from bilateral hip prostheses during lower extremity computed tomography angiography: an experimental phantom study

Omarah N. Abdalqader, MSc[1], Mohammad Hjouj, PhD[1], Mohammad Aljamal, PhD[2], Fawaz Hjouj, PhD[3], Mohamed Abuzaid, PhD[4], & Mahmoud Mousa, MSc[5]

[1]Department of Medical Imaging, Faculty of Health Professions, Al-Quds University, Jerusalem, Palestine
[2]Department of Medical Imaging, Faculty of Allied Medical Sciences, Arab American University, Jenin, Palestine
[3]Department of Mathematics, Khalifa University, Abu Dhabi, UAE
[4]Medical Diagnostic Imaging Department, College of Health Sciences, University of Sharjah, Sharjah, UAE
[5]Department of Radiology, Turkish Friendship Hospital, Gaza Strip, Palestine

Keywords
CT metal artefacts, iterative model-based reconstruction, lower extremity CT angiography, metal artefact reduction, O-MAR

Correspondence
Mohammad Aljamal, Department of Medical Imaging, Faculty of Allied Medical Sciences, Arab American University, P.O Box 240, Jenin, 13 Zababdeh, Palestine. Tel: +00970-59-7259916; fax: +00970-4-2510810; E-mail: mohammad.aljamal@aaup.edu

Received: 20 December 2023; Accepted: 1 May 2024

J Med Radiat Sci **0** (2024) 1–11

doi: 10.1002/jmrs.797

Abstract

Introduction: Image quality reduction due to metallic artefacts is a significant challenge during vascular computed tomography (CT) imaging of the lower extremities in patients with hip prostheses. This study aims to analyse various reconstruction algorithms' ability to reduce metal artefacts due to two types of hip prostheses during lower extremity CT angiography examinations. **Methods:** A pelvis phantom was fabricated with the insertion of a tube filled with contrast media to simulate the femoral artery, and the phantom was then CT scanned with and without hip prostheses. Multimodal images were acquired using different kilovoltage peak (kVp) settings and reconstructed with different algorithms, such as filtered back projection (FBP), iterative reconstruction (iDose^4), iterative model-based reconstruction (IMR) and orthopaedic metal artefact reduction (O-MAR). Image quality was assessed based on image noise, signal-to-noise ratio (SNR) and Hounsfield unit (HU) deviation. **Results:** The IMR approach significantly improved image quality compared to iDose^4 and FBP. For the vascular region, O-MAR improves SNR by 5 ± 1, 23 ± 5 and 42 ± 9 for FBP, iDose^4 and IMR respectively, and improves HU precision towards the baseline values by 49% and 83% for FBP and IMR, respectively. The noise reduction was 71% and 89% for FBP and IMR, and 57% for iDose^4. O-MAR greatly enhances SNR corrections among the most severe artefacts, with 29 ± 1 and 43 ± 4 for FBP and IMR, compared to iDose^4 by 37 ± 7. **Conclusion:** IMR combined with O-MAR could improve the CT angiography of the lower extremities of patients with a hip prosthesis.

Introduction

Lower extremity peripheral artery disease (PAD), a chronic arterial occlusive disease of the lower limbs caused by atherosclerosis, one of the key pathogenic factors in cardiovascular disease, is caused by this occlusion. In conjunction with this, it also contributes to cardiovascular deaths and morbidity and poses a serious healthcare issue. 12% to 20% of Americans aged 60 and older suffer from lower extremity peripheral arterial disease (PAD), which rises to over 50% in those aged 85 and beyond.[1] At the same time, the number of primary total hip arthroplasty (THA) procedures performed annually in the United States is predicted to increase from 511,000 by 2020 to 572,000 by 2030.[2] Up to 42% of the population with osteoarthrosis may experience bilateral hip disease,[3] and it is predicted that 25% of individuals with osteoarthritis also require bilateral hip replacement.[4] Thus, older people are more susceptible to the occurrence of PAD, and at the same time, the patient needs to replace one hip joint or both hips due to degenerative hip osteoarthritis.

Computed tomography angiography (CTA) has shown a diagnostic performance comparable to digital subtraction angiography (DSA) due to its speed and accuracy in evaluating peripheral artery disease.[5] However, there is a challenge during the CTA of the lower extremity, which is the metal artefact induced by hip prostheses. This would significantly affect the image quality of vascular CT imaging, particularly in lower extremity diagnoses of the internal and external iliac arteries. The resulting poor image quality is due to photon starvation, scattering and beam hardening.[6,7] Therefore, various techniques have been used to reduce metal artefacts in CT images and to improve the image quality, including metal artefact reduction (MAR). The metal artefact reduction technique focuses on fixing or minimising artefacts in projection or image data.[8] Philips has developed an O-MAR algorithm to minimise metal artefacts in CT scans of large metal implants.[9] It uses a combination of projection adjustments to increase contrast-to-noise ratios (CNR) and correct the deviations in CT numbers to improve image quality.[10] Its capacity to overcome artefacts, however, is predicated on reconstruction methods that have been combined, such as filtered back projection (FBP), iterative reconstruction (IR), iDose[4] or model-based iterative reconstruction (MBIR) algorithms.[11] Nevertheless, O-MAR has not been evaluated before with combinations of the mentioned reconstructed algorithms to reduce the apparent artefacts resulting from a single or bilateral hip replacement in a patient undergoing lower extremity CT angiography (CTA). Therefore, this study aims to investigate the efficacy of O-MAR integration with FBP, IR, iDose[4] and IMR algorithms in enhancing image quality and minimising metal artefacts due to hip prostheses replacement for patients undergoing lower extremity CT angiography imaging.

Materials and Methods

Fabrication of pelvic phantom

A custom-designed phantom was fabricated to simulate the adult human pelvis, measuring $32 \times 38 \times 25$ cm. It comprises four main components: pelvis bones, fat, muscle tissue and vascular structures, as visually depicted in Figure 1A. Fabrication of these components involved utilising diverse chemical materials characterised by distinct densities and specified concentrations. A plastic with calcium sulphate ($CaSO_4$), bee wax mixed with water, agarose with water and Iohexol contrast medium with water were made instead of bone, fat, muscle tissue and vascular structure, respectively, as outlined in Table 1. Before fabrication, each component in the phantom was tested to achieve a suitable concentration with the closest Hounsfield units of targeted tissues. Therefore, each material mentioned above was prepared separately with different concentrations and filled in a 100-mL container made of a low-attenuating material made of polyethylene. The samples were then tested using CT scanning (Philips Brilliance 128-slice scanner) based on the measurement of CT numbers quantified in Hounsfield units (HU). The HU value was measured by drawing a region of interest (ROI) of a 40-pixel circular shape on a CT image of each material. The HU values obtained for each material accurately mirrored the density characteristics of human pelvis structures. The HU ranges used as references were 250 to 1000 HU for bone,[12] −29 to 150 HU for muscle tissue,[13] −200 to 10 HU for fat[14] and 200 to 600 HU for vascular structure.[15] The average HU values obtained in this study were as follows: bone (900 HU), muscle (26 HU), fat (−90 HU) and vascular structures (400 HU). After obtaining the suitable HU for materials based on the concentration in Table 1, three

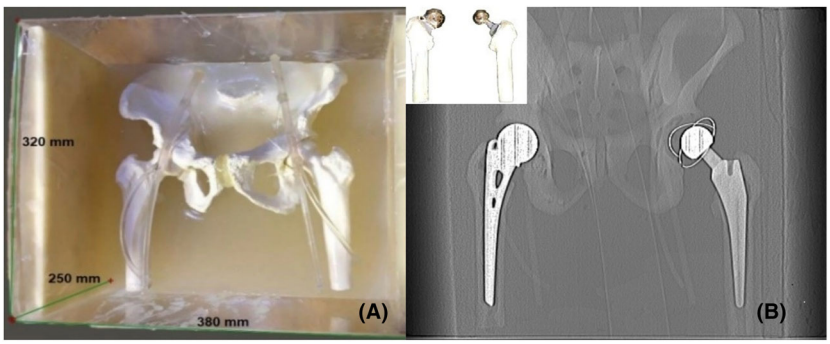

Figure 1. (A) Fabricated pelvis phantom without a hip prosthesis. (B) Scout CT image after insertion of two types of hip prostheses: a 40-mm head metal on cemented cup total hip prosthesis and the standard neck with a titanium-aluminium–vanadium (Ti-6Al-4V) stem inserted in the left femur. A 46-mm Austin Moore hip prosthesis was used for the right femur.

Table 1. The materials used to fabricate pelvis phantoms include bone, muscle tissue, fat and vessels.

Tissue	Components
Bone	26% calcium sulphate ($CaSO_4$) and 74% distilled water
Fat	89% bee wax and 11% distilled water
Muscle	3% agarose powder; 97% distilled water and 2 mL Iohexol contrast medium
Vascular structures	3% Iohexol and 97% distilled water

samples of each material were prepared, and then they were tested again using a CT scan to check the validity and reliability of the measurements obtained. After obtaining the requested HU value, two phantoms were fabricated, one without hip prostheses as a reference and the other with hip prostheses. The averaged HU values measured in the fabricated reference pelvic phantom are shown in Table S1. A low-attenuation polyethylene tube was used to simulate the femoral artery with a diameter of 0.52 cm, which is the femoral artery's average diameter measured below the femoral head's inferior border.[16] These materials were judiciously chosen to emulate the anatomical features of the adult human pelvis while ensuring compatibility with computed tomography (CT) imaging.

Two types of hip prostheses were used in this study, commonly employed for treating femoral neck fractures in both elderly and younger patients,[9,17] as delineated in Figure 1B. The first variant consisted of a 40 mm head metal-on-cemented-cup total hip prosthesis, featuring a standard neck design (Biomet Ltd., UK) and implanted with a titanium-aluminium-vanadium (Ti-6Al-4 V) stem within the left femur. In contrast, the second variant incorporated a 46 mm head metal-on-metal Austen Moore Prosthesis composed of stainless steel alongside a standard stem, which was utilised for the right femur.

Study design, image acquisitions and reconstructions

CT scans were performed with and without inserting the hip prosthesis into the fabricated phantom using a Philips Brilliance CT 128-slice scanner. Since the X-ray tube voltage significantly impacts the CT image quality and radiation dose of a patient, particularly in high-attenuation material, all images were obtained using FBP reconstruction with different kVp settings of 80, 100, 120 and 140 kVp. At the same time, milliampere seconds (mAs) were fixed to 250 mAs based on the clinical setting for imaging the average adult patients. Hence, eight separate FBP reconstructions were made from CT scans with and without the prosthesis using various kVp settings. The CT images were reconstructed separately using iDose4 and iterative model base reconstruction (IMR) without O-MAR. For optimal contrast and reasonable evaluation, iDose^4 level 4 and IMR Level 2 were applied, as they are the middle levels of noise reduction. The O-MAR algorithm was then applied to each reconstruction algorithm individually for comparison purposes with those obtained without O-MAR. The CT images without prostheses were used as reference images to determine the derived values. All images were scanned using 64×0.625 mm collimation parameters, 1.5 mm slice thickness with 1.0 mm increment, 460 mm field of view, 0.524 pitch and 0.5 s rotation time. A strong or sharp filter was selected to improve contrast and reinforce the edges between hard and soft objects. As a consequence, the sharp filter D has been used for FBP and iDose4, while the filter Sharp Plus was used for IMR.

Data analysis

Various regions of interest (ROIs) were carefully examined to assess the image quality and extent of metal artefacts and to evaluate the effectiveness of metal artefact reduction in targeted regions. The ROIs denoted as (R1–R5) were manually delineated, as depicted in Figure 2, based on single axial slices obtained for each energy kilovolt peak (kVp) scan. These ROIs corresponded to specific anatomical structures: the right and left common femoral arteries, the right gluteus medius muscle, adipose tissue and the urinary bladder, respectively, spanning from R1 to R5. The diameter of regions R1 and R2 was 30 pixels to cover the vascular area, while regions R3 and R5 possessed a diameter of 360 pixels. This deliberate

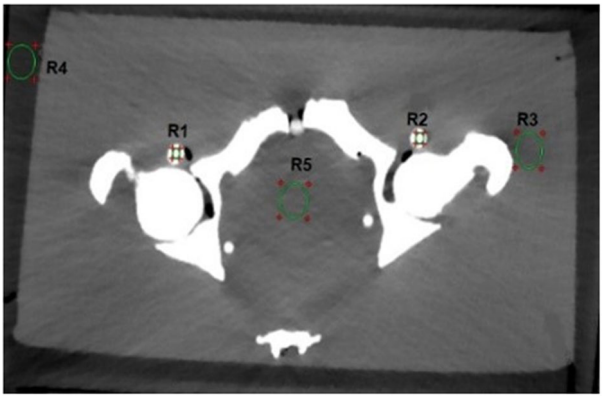

Figure 2. The axial CT slice of the fabricated pelvis phantom shows various RIOs (R1–R5) without hip prostheses.

selection minimised partial volume effects across all regions and ensured that it was positioned at the central portion of the artefact. MATLAB Toolbox Release 2014b software was employed as the computational tool for CT image quantitative analysis. Averaged Hounsfield Unit (HU) values, noise levels and signal-to-noise ratios (SNRs) were used as assessment parameters to analyse image improvement in ROIs. ROIs within each slice were considered, with their mean HU values serving as representative attenuation indicators. The standard deviation within each ROI was employed to quantify the noise level. SNRs were calculated by dividing the average HU values by the respective noise levels. Consequently, the correction of metal artefacts through the utilisation of metal artefact reduction in the vascular regions and other selected surrounding regions was evaluated by applying the following equations[18]:

$$\text{Deviation}_{\text{without O-MAR}} = \text{Reference value–value without O-MAR}|$$

$$\text{Deviation}_{\text{with O–MAR}} = \text{Reference value–value with O} - \text{MAR}$$

$$\text{Correction by O–MAR}(\%) = (1-(\text{Deviation}_{\text{with O–MAR}} / \text{Deviation}_{\text{without O–MAR}})) \times 100$$

The statistical analysis was carried out using the Minitab® statistical software. Descriptive statistical methods, such as percentages, means and charts, were applied to compare the performance of different algorithms under various conditions and assumptions. It utilised a *t*-test comparing two independent population means with unknown and possibly unequal population standard deviations. A value of $P < 0.05$ was used as a significance standard.

Results

Without insertion of hip prosthesis

For CT image analysis without using hip prostheses, IMR showed lower deviation in HU values, better SNRs ($P < 0.05$) and lower noise values ($P < 0.001$) in comparison with FBP and iDose[4] for regions R1–R5, as shown in Table S1.

With the insertion of the prosthesis

The hip phantom prosthesis affected four regions of interest (R1, R2, R3 and R5) at different levels. Region R5 was most severely affected, and R4 was identified as the unaffected area. In contrast, a mild artefact effect was seen in regions R2 and R3. Region R1 was affected by a white streak artefact because it was located close to a high-density head prosthesis. As a result, regions R1 and R5 were the primary areas with high metallic artefacts. The CT images with and without using O-MAR reconstruction techniques are shown in Figure 3.

CT image evaluation

In the CT images evaluated after the insertion of hip prostheses and without using O-MAR, the SNRs decreased and noise values increased compared to

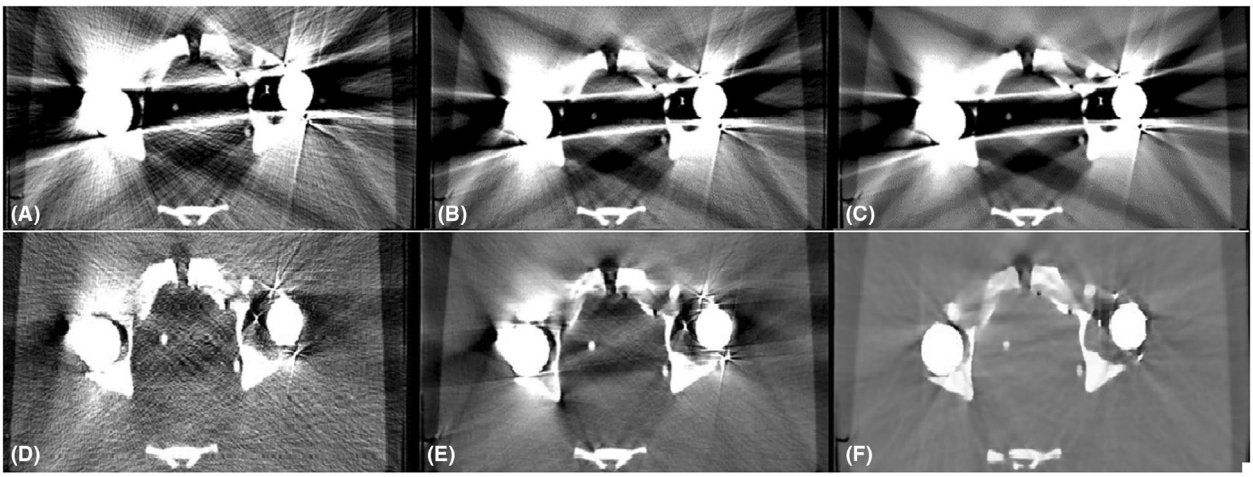

Figure 3. 140-kVp images were reconstructed using different algorithms with and without O-MAR. (A) the reconstructed images obtained with FBP without O-MAR, (B) the reconstructed images obtained with iDose4 without O-MAR, (C) the reconstructed images obtained with IMR without O-MAR, (D) using FBP with O-MAR, (E) using iDose4 with O-MAR and (F) using IMR with O-MAR.

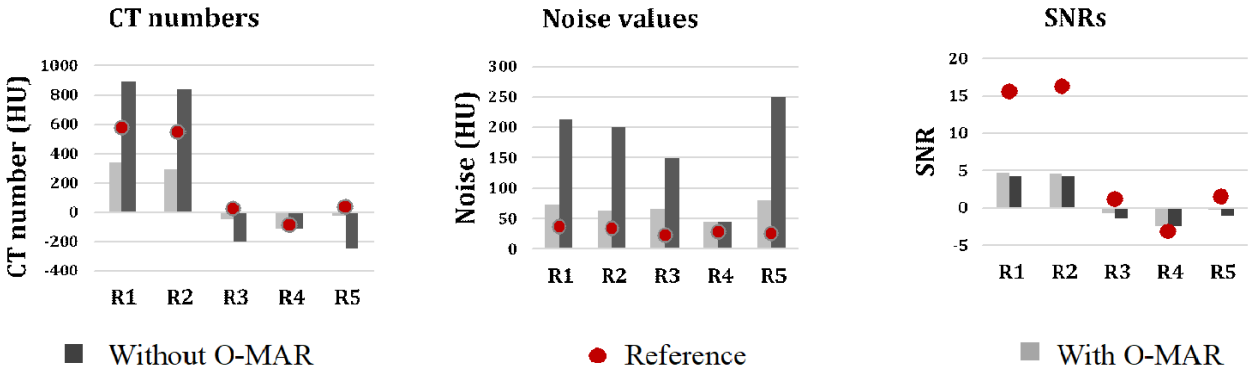

Figure 4. CT numbers (HU), noise values and SNRs for regions (R1–R5) with and without O-MAR at 120 kVp reconstructed with FBP after prosthesis insertion. The reference values are shown in red in the absence of the prosthesis.

reference values due to metal artefacts for all regions (Fig. 4). HU values decreased for regions R3 and R5 but increased for regions R1 and R2 (vascular regions) because they were affected by white streak artefacts. In contrast, the usage of O-MAR reduces HU value variations in regions R1, R2, R3 and R5 from baseline values, and it was most noted in regions R1 and R5. The HU values of region R4 were equivalent despite the application of O-MAR because it was unaffected by metal artefacts since it was beyond the prosthesis's scan area. The SNR of region R5 was lower, obliterating the boundary between region R5 and the adjacent tissue as it is located between the two prosthesis heads and affected by a black streak artefact. On the other hand, the SNR of region R1 was less than the reference value without insertion of the prosthesis, eliminating the boundaries across region R1, since it was affected by a white streak artefact due to high-density prosthesis.

O-MAR performed better in correcting these deviations when it was paired with IMR with total SNR corrections in region R1 by 5 ± 1, 23 ± 5 and 42 ± 9 for FBP, iDose^4 and IMR, respectively ($p < 0.05$) (Table S2, Fig. 5). O-MAR greatly enhanced SNR corrections among the most severe artefacts in region R5, with 29 ± 1 and 43 ± 4 for FBP and IMR ($p < 0.05$), compared to iDose^4 by 37 ± 7 without any significant changes ($p < 0.05$) (Table S3, Fig. 6). Although O-MAR could not return SNRs to the reference values of unaffected regions R4, a great visual improvement was observed when paired with IMR, as shown in Figure 4. On the other hand, for region R1, O-MAR efficiency showed little variation when paired with IMR and for the 80 and 140-kVp results regarding SNRs (Table S2). O-MAR paired with IMR yielded HU corrections of 90%, 68%, 81% and 93% for the lowest and highest photon energy settings, respectively. The noise was corrected with 89%, 88%, 90% and 89% for the same energy level. For findings at 80, 100, 120 and 140 kVp, respectively, SNR adjustments were 55%, 42%, 38% and 34%, respectively.

Regarding addressing severe artefacts in region R5, O-MAR was most successful when paired with 140-kVp performance and IMR. For region R5, OMAR paired with IMR revealed HU corrections of 90%, 90%, 93% and 93% for 80, 100, 120 and 140 kVp settings. Noise values were adjusted with 92%, 91%, 92% and 92% for 80, 100, 120 and 140 kV settings, respectively. SNR corrections were 37%, 38%, 46% and 52% for 80, 100, 120 and 140 kVp results, respectively (Table S3).

Discussion

In this phantom research, we investigated the utility of several reconstruction techniques to assess their ability to eliminate metallic artefacts due to two types of hip prostheses and their effect on lower extremity CT angiography examinations. Several approaches for decreasing metal artefacts have been presented, including O-MAR and model-based iterative reconstruction (MBIR) termed IMR (Philips), which might combine both techniques. We confirmed that O-MAR with IMR can effectively lower metal artefacts even if induced due to bilateral hip prostheses at a range of tube voltages of 80–100 kVp and enhance vascular visibility.

CTA is a well-known modality in the diagnostic assessment of cardiovascular disease with accuracy comparable to that of angiography.[19] CTA has many potential benefits over traditional angiography, such as being less invasive, widely available and having high diagnostic accuracy. In contrast, the risk of complications from traditional angiography is high, particularly in elderly patients. However, radiation exposure from CTA is still a major concern for radiology staff.[20] Additionally,

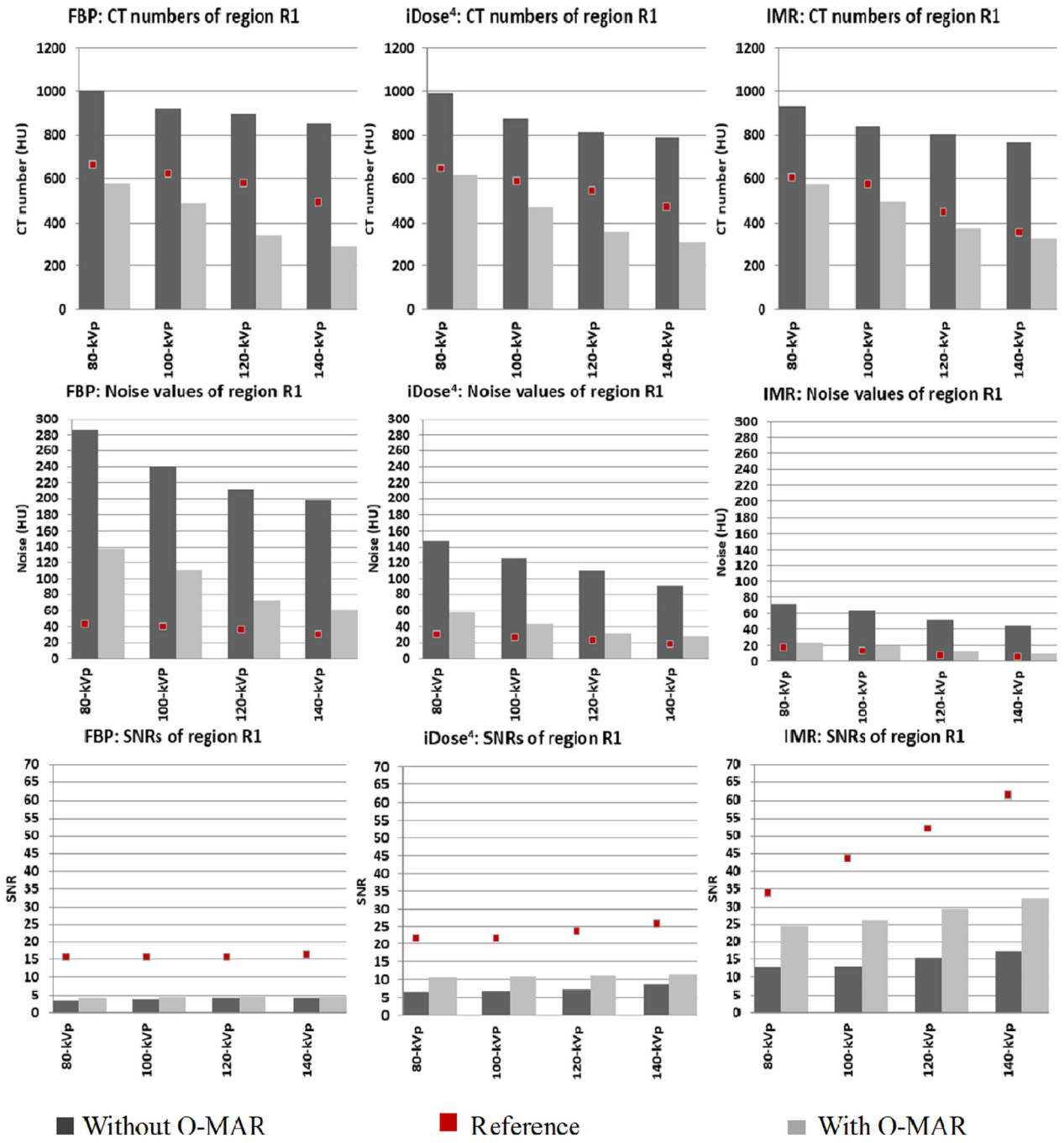

Figure 5. The CT numbers (HU values), noise values and SNRs in severe metal artefacts in the right vascular region (R1) for different kVp settings utilising FBP, iDose4 and IMR. The reference values are shown in red in the absence of the prosthesis.

due to its complicated acquisition settings and extensive scanning duration, it is one of the most significant sources of radiation dose among all CT approaches. Moreover, research indicates that the gender of the patient has a significant difference in responding to the risk of radiation dose, with females being more prone to radiation-induced malignancies than males.[21] Therefore, female patients who undergo CTA examinations are exposed to a higher risk of radiation compared to male patients. The concern becomes greater if the woman is scanned with this examination in areas with sensitive structures, such as the pelvic area during CTA of the

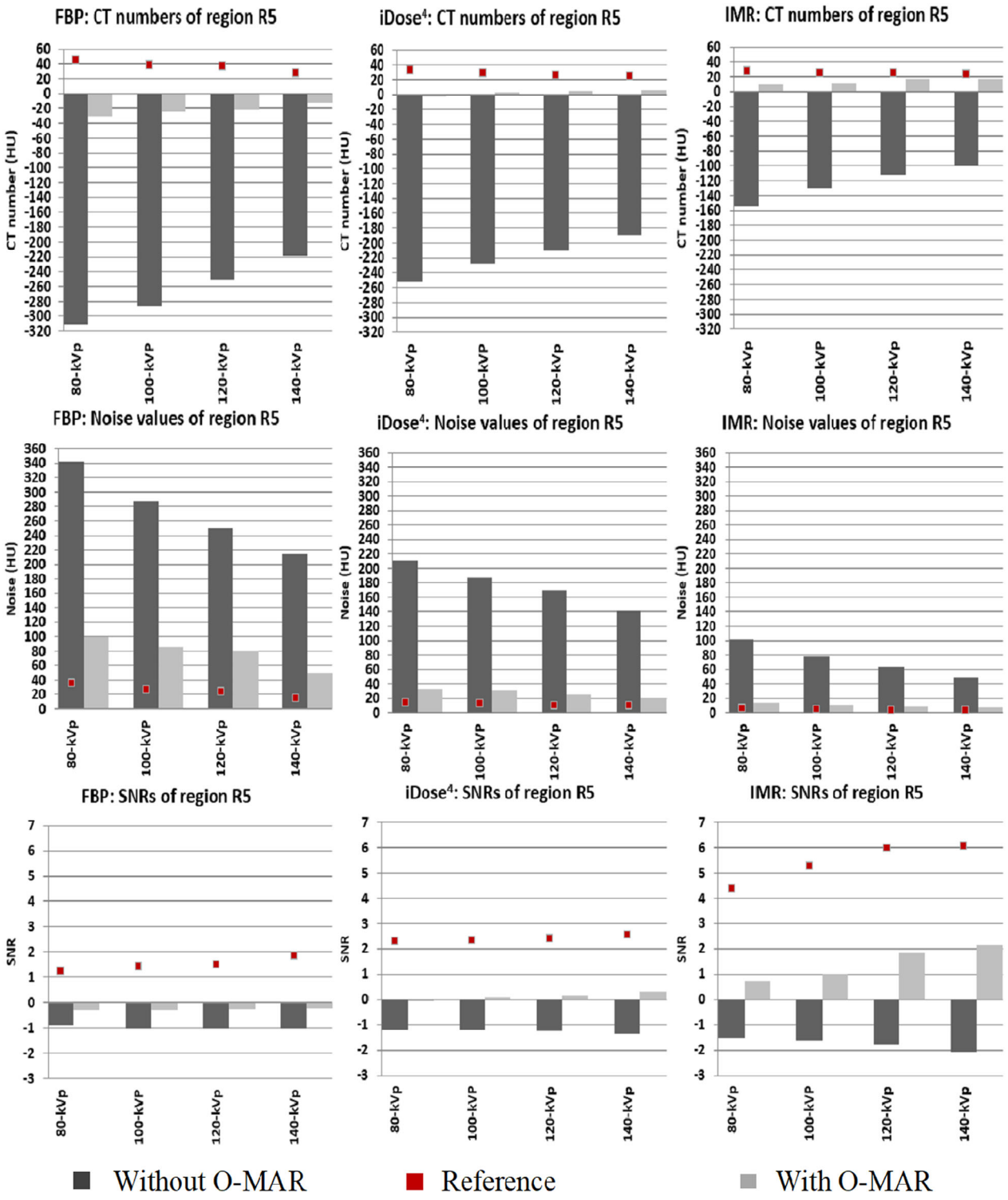

Figure 6. The CT numbers (HU values), noise values and SNRs in severe metal artefacts in region R5 at 80, 100, 120 and 140 kVp processed using FBP, iDose4 and IM¬R. The reference values are shown in red in the absence of the prosthesis.

lower extremity, where the uterus is considered a sensitive organ to radiation. Subsequently, the patients and technologists are both prone to psychological disorders of worry, discomfort and depression during CTA examinations; the patients have mostly phobias of radiation, which leads to an increased heart rate.[22] The staff also has a phobia of the chance of repeating CT exams due to poor imaging quality,[23] including the artefacts resulting from hip prostheses. Thus, the radiation technologist should optimise radiation dosage during CTA examinations, an essential factor in reducing the radiation dose to patients. One of the methods used to reduce radiation dose for patients is the use of reconstruction algorithms, especially in the presence of metallic artefacts due to the presence of a hip prosthesis, to reduce the chances of a rescan of the patient and improve image quality.[24]

It was obvious that there was a variation in the capabilities of each reconstruction algorithm to improve the image quality based on the values obtained from the analysed CT image of the phantom, particularly without using a hip prosthesis. The IMR algorithm dramatically reduces noise levels in all-tube voltage settings compared to conventional FPB and iDose^4. Moreover, IMR enhanced image quality with higher SNRs than FPB and iDose^4 (Table S1). It can also handle the higher noise levels typically associated with traditional and iterative reconstruction methods. These techniques have commonly used the combination of system models of both data and image statistics to improve the algorithm's performance.[25] However, IMR had lower HU values relative to FBP and iDose^4. This could be attributed to variations in kernel kind; the sharp kernel uses edge enhancement to enhance the interface between structures, which leads to the effect of the computed tomography numbers (HU) of small structures.[26]

After the insertion of hip prostheses, metal artefacts exhibit deviations in the mean values of noise, HU and SNRs in most regions. This effect was clear in the middle area between the two prostheses (R5) and the right vascular region (R1). R5 was the most profoundly affected region since it was placed between the prosthetic heads. The right vascular region was affected distinctly due to its placement close to a high-density stainless-steel head prosthesis compared to the left vascular region near the hip implant made of titanium vanadium. Titanium material produces fewer streak artefacts in CT images due to its lower mass attenuation coefficient properties.[27] Despite this, it is undeniable that this type of prosthesis makes diagnosis difficult for certain diseases.[28] On the other hand, the prosthesis on the right side presents a high metallic artefact on the CT image, which hides the tube filled with contrast media. This type of prosthesis is still used in some countries because of its distinctive characteristics, such as its physical and mechanical properties.[29] This shows without a doubt that the type of hip prosthesis has a significant effect on the CT image; stainless steels produce a high metallic artefact compared to titanium; hence, the selection of a proper reconstruction algorithm is crucial in removing the metallic artefact induced.

Integration of O-MAR and IMR for CT images, particularly in the vascular region (R1), with high metallic artefacts resulted in a significant correction in deviated SNRs. However, there was no significant difference in noise or HU value (Fig. 5). Still, this combination of O-MAR and IMR showed the best image quality compared to other combinations. This could be explained by the fact that the IMR algorithm can better correct the missing information, which continuously delivers consistent and predictable attenuation profiles in the final image. Therefore, this vascular region was successfully treated with this type of technique. Kuya et al. revealed that IMR significantly reduced the size of the artefacts surrounding the implant compared to FBP.[30] Another study revealed that using MBIR, a type of IMR technique, reduced streak artefacts and improved overall image quality.[31] O-MAR had a good impact on intermediate artefacts concerning HU values, with slight HU differences in most cases for the left vascular region (R2) and the region close to the femur head (R3). HU values, noise values and SNRs of regions outside the metallic artefact, such as in our case R4, verified that O-MAR would not change the values in those regions.[25] Boomsma et al. noted that the absence of metal artefacts in the unaffected area allows for a more accurate diagnosis ability to assess bone mineral density in CT of the acetabular region, which may be employed in total hip surgical repair.[32] O-MAR reduced HU differences in severe metal artefacts, influencing the region at all reconstruction algorithms and tube voltages. In addition, O-MAR minimised noise and increased SNRs in other impacted regions. The effectiveness of O-MAR varied depending on the IR technique, but when paired with IMR, it considerably increased in effectiveness. This is consistent with a previous study by Wellenberg et al., which concluded that using O-MAR with MBIR can reduce artefacts resulting from hip prostheses.[11]

The O-MAR algorithm identifies and corrects data distorted by streak artefacts using uncorrupted projection data.[18] IMR may be used to remove image noise, producing an image free of artefacts and noise.[33] Therefore, the combination of these two reconstructions reduced the number of metal artefacts. In contrast, FBP itself couldn't effectively manage the noise due to metal artefacts, especially in severe artefacts, where the total

noise values recorded were high using FBP and only moderately decreased, even with O-MAR.[25] The integration of O-MAR and IMR resulted in a significant noise reduction. Even using a low tube voltage of 80 keV showed a good contribution to better noise reduction than iDose[4] and FBP in vascular regions (Fig. 5). This is attributed to the fact that O-MAR has shown usefulness even at lower tube voltages due to specific metal separation and tissue segmentation at low tube voltages.[34] This is consistent with a study by Boomsma et al., who reported that O-MAR can improve the contrast-to-noise ratio (CNRs) even with lower tube voltage.[18] It has also been shown that IMR can reduce noise and improve image quality in low tube acquisition while minimising radiation dose.[35] Nevertheless, the excessive reduction in noise in low-dose acquisitions may result in image blurring, resolution degradation and over-smoothing of the image.[36]

It was also found that using the combination of IMR and O-MAR with 120 and 140 kVp was successful in metal artefact reduction with lower noise and better SNR in the case of severe metal artefacts. Using a higher tube voltage of 140 kVp that penetrates metal with higher-energy x-ray beams reduces both the beam-hardening effect and the statistical noise.[37] It supports O-MAR in reducing metal artefacts and noise correction.[38] A previous study stated that integrating IMR and O-MAR with 140 kVp significantly increased the overall image quality and was the most efficient in reducing metal artefacts.[25] However, a tube voltage of 140 kVp will increase the radiation dose to 30.8 mGy.[38] The vascular region's relative SNRs improved with O-MAR by 55% and 34% when paired with the IMR algorithm at tube voltages of 80 and 140 keV, respectively (Table S2). Reducing the kVp setting can improve the enhancement of the vessels in CT angiography. Based on the values obtained in our study, it is recommended that employing an 80–100 kVp rather than a 120–140 kVp is an important means for greater contrast and compromise between improving image quality in the vascular region and, at the same time, being able to remove metallic artefacts. Our results are consistent with a recent study in 2023, which concluded that the 70–80 keV range had higher diagnostic interpretation scores in peripheral arterial disease evaluation that included metal artefacts.[39]

Moreover, using a low tube voltage causes an increase in the intrinsic attenuation as it is close to the K-edge energy of 33.2 kilo electron volts (keV) due to the high atomic number of iodine contributing to the increase in the overall signal.[40] Another study by Zhao et al. reached the same results, and this is attributed to the fact that the vessel with contrast media undergoes a photoelectric effect to appear clearly in CT images.[41] An analysis by Fan Zhang et al. revealed that using an 80 kVp setting and IMR could improve the quality of images by reducing noise and artefacts.[33] This finding is probably due to IMR's ability to boost low- and high-contrast detectability by reducing image noise and artefacts, and using a low-kVp setting could help boost vascular structure enhancement. In addition, as mentioned earlier, O-MAR delivers more consistent attenuation, potentially increasing the overall efficiency of IMR.[30] Woo et al. reported that O-MAR enhances the image quality, vascular conspicuity and noise of lower limb CT venography in patients with metallic hip or knee prostheses.[42]

The findings of this study suggest a practical strategy for improving the quality of CT imaging due to hip prostheses during a lower extremity CTA examination based on a phantom study. To the authors' knowledge, this is the first study that has simulated vascular imaging of the lower extremity with two existing hip prostheses. However, some limitations exist in this investigation. First, the study used a single system (128-row Philips CT scanner) with a fixed tube current; hence, the results may not be directly comparable to those of other manufacturers. Future research should incorporate the scanner and tube current effect reliance into their outcomes. Second, subjective image analysis of patients with vascular disease is needed to evaluate the diagnostic value. Finally, the limitation of the study revolves around not examining the impact of reconstruction algorithms on the precision of blood vessel reproduction and the diagnostic implications of artefacts. This oversight is significant as it pertains to the accuracy of diagnoses in patients with bilateral hip prostheses undergoing lower extremity CT angiography. Addressing this limitation involves acknowledging the potential influence of reconstruction techniques on diagnostic outcomes, suggesting a direction for future research to explore these effects further.

In conclusion, to improve the quality of CT imaging of a total hip prosthesis during CTA of the lower extremity examination, the integration of IMR and O-MAR is an efficient method, even with high-density hip prostheses. It would also provide a valuable tool for diagnosing vascular diseases in patients with total hip replacement. It is indicated that using an 80–100 kVp is an essential technique for increasing contrast and achieving a balance between boosting CT image quality in the vascular region and reducing metallic artefacts.

Conflict of Interest Statement

The authors declare no conflict of interest.

Ethics Statement

Quality improvement project was granted exemption from full ethics approval by an institutional ethics officer.

Data Availability Statement

The data that support the findings of this study are available from the corresponding author upon reasonable request.

References

1. Benjamin EJ, Virani SS, Callaway CW, et al. Heart Disease and Stroke Statistics-2018 Update: A Report From the American Heart Association. *Circulation* 2018; **137**: e67–e492.
2. Kurtz S, Ong K, Lau E, Mowat F, Halpern M. Projections of primary and revision hip and knee arthroplasty in the United States from 2005 to 2030. *J Bone Joint Surg Am* 2007; **89**: 780–5.
3. Stavrakis AI, SooHoo NF, Lieberman JR. Bilateral total hip arthroplasty has similar complication rates to unilateral total hip arthroplasty. *J Arthroplasty* 2015; **30**: 1211–4.
4. Lorenze M, Huo MH, Zatorski LE, Keggi KJ. A comparison of the cost-effectiveness of one-stage versus two-stage bilateral total hip replacement. *Orthopedics* 1998; **21**: 1249–52.
5. Kosmala A, Weng AM, Schmid A, et al. Dual-Energy CT angiography in peripheral arterial occlusive disease: diagnostic accuracy of different image reconstruction approaches. *Acad Radiol* 2022; **29**(Suppl 4): S59–68.
6. Katsura M, Sato J, Akahane M, Kunimatsu A, Abe O. Current and novel techniques for metal artifact reduction at CT: practical guide for radiologists. *Radiographics* 2018; **38**: 450–61.
7. Mori I, Machida Y, Osanai M, Iinuma K. Photon starvation artifacts of X-ray CT: their true cause and a solution. *Radiol Phys Technol* 2013; **6**: 130–41.
8. Wellenberg RH, Boomsma MF, van Osch JA, et al. Computed tomography imaging of a hip prosthesis using iterative model-based reconstruction and orthopaedic metal artefact reduction: a quantitative analysis. *J Comput Assist Tomogr* 2016; **40**: 971–8.
9. Kidoh M, Nakaura T, Nakamura S, et al. Reduction of dental metallic artefacts in CT: value of a newly developed algorithm for metal artefact reduction (O-MAR). *Clin Radiol* 2014; **69**: e11–6.
10. Shim E, Kang Y, Ahn JM, et al. Metal artifact reduction for orthopedic implants (O-MAR): usefulness in CT evaluation of reverse total shoulder arthroplasty. *AJR Am J Roentgenol* 2017; **209**: 860–6.
11. Wellenberg RH, Boomsma MF, van Osch JA, et al. Low-dose CT imaging of a total hip arthroplasty phantom using model-based iterative reconstruction and orthopedic metal artifact reduction. *Skeletal Radiol* 2017; **46**: 623–32.
12. Glorieux FH, Pettifor JM, Jüppner H. Pediatric Bone Biology and Diseases, 2nd edn. Amsterdam, Netherlands: Elsevier Science, 2011.
13. van der Werf A, Langius JAE, van der Schueren MAE D, et al. Percentiles for skeletal muscle index, area and radiation attenuation based on computed tomography imaging in a healthy Caucasian population. *Eur J Clin Nutr* 2018; **72**: 288–96.
14. Edmunds KJ, Gíslason MK, Arnadottir ID, Marcante A, Piccione F, Gargiulo P. Quantitative Computed Tomography and Image Analysis for Advanced Muscle Assessment. *Eur J Transl Myol* 2016; **26**: 6015.
15. Manniesing R, Velthuis BK, van Leeuwen MS, van der Schaaf IC, van Laar PJ, Niessen WJ. Level set based cerebral vasculature segmentation and diameter quantification in CT angiography. *Med Image Anal* 2006; **10**: 200–14.
16. Spector KS, Lawson WE. Optimizing safe femoral access during cardiac catheterization. *Catheter Cardiovasc Interv* 2001; **53**: 209–12.
17. Pluot E, Davis ET, Revell M, Davies AM, James SL. Hip arthroplasty. Part 1: prosthesis terminology and classification. *Clin Radiol* 2009; **64**: 954–60.
18. Boomsma MF, Warringa N, Edens MA, et al. Quantitative analysis of orthopedic metal artefact reduction in 64-slice computed tomography scans in large head metal-on-metal total hip replacement, a phantom study. *Springerplus* 2016; **5**: 405.
19. Sabarudin A, Siong TW, Chin AW, Hoong NK, Karim MKA. A comparison study of radiation effective dose in ECG-Gated Coronary CT Angiography and calcium scoring examinations performed with a dual-source CT scanner. *Sci Rep* 2019; **9**: 4374.
20. Karim MKA, Hashim S, Bradley DA, Bahruddin NA, Ang WC, Salehhon N. Assessment of knowledge and awareness among radiology personnel regarding current computed tomography technology and radiation dose. *J Phys: Conf Ser* 2016; **694**: 012031.
21. Council NR. Health Risks from Exposure to Low Levels of Ionizing Radiation: BEIR VII Phase 2. The National Academies Press, Washington, DC, 2006; 422.
22. Heyer CM, Thüring J, Lemburg SP, et al. Anxiety of patients undergoing ct imaging—an underestimated problem? *Acad Radiol* 2015; **22**: 105–12.
23. Paalimäki-Paakki K, Virtanen M, Henner A, Nieminen MT, Kääriäinen M. Patients', radiographers' and radiography students' experiences of 360° virtual counselling environment for the coronary computed tomography angiography: A qualitative study. *Radiography* 2021; **27**: 381–8.
24. Kawahara D, Ozawa S, Yokomachi K, et al. Metal artifact reduction techniques for single energy CT and dual-energy CT with various metal materials. *BJR Open* 2019; **1**: 20180045.
25. Wellenberg RH, Boomsma MF, van Osch JA, et al. Quantifying metal artefact reduction using virtual monochromatic dual-layer detector spectral CT imaging in

unilateral and bilateral total hip prostheses. *Eur J Radiol* 2017; **88**: 61–70.
26. Narita A, Ohkubo M. A pitfall of using the circular-edge technique with image averaging for spatial resolution measurement in iteratively reconstructed CT images. *J Appl Clin Med Phys* 2020; **21**: 144–51.
27. Winklhofer S, Hinzpeter R, Stocker D, et al. Combining monoenergetic extrapolations from dual-energy CT with iterative reconstructions: reduction of coil and clip artifacts from intracranial aneurysm therapy. *Neuroradiology* 2018; **60**: 281–91.
28. Shinohara Y, Ohmura T, Sasaki F, Inomata T, Itoh T, Kinoshita T. Appropriate iMAR presets for metal artifact reduction from surgical clips and titanium burr hole covers on postoperative non-contrast brain CT. *Eur J Radiol* 2021; **141**: 109811.
29. Alireza Nouri CW. 3 - Stainless steels in orthopedics. *Struct Biomat* 2021; **10**: 67–101.
30. Kuya K, Shinohara Y, Kato A, Sakamoto M, Kurosaki M, Ogawa T. Reduction of metal artifacts due to dental hardware in computed tomography angiography: assessment of the utility of model-based iterative reconstruction. *Neuroradiology* 2017; **59**: 231–5.
31. Yasaka K, Katsura M, Akahane M, Sato J, Matsuda I, Ohtomo K. Model-based iterative reconstruction for reduction of radiation dose in abdominopelvic CT: comparison to adaptive statistical iterative reconstruction. *Springerplus* 2013; **2**: 209.
32. Boomsma MF, Slouwerhof I, van Lingen C, et al. CT-based quantification of bone stock in large head metal-on-metal unilateral total hip replacements. *Eur J Radiol* 2016; **85**: 760–3.
33. Zhang F, Yang L, Song X, et al. Feasibility study of low tube voltage (80 kVp) coronary CT angiography combined with contrast medium reduction using iterative model reconstruction (IMR) on standard BMI patients. *Br J Radiol* 2016; **89**: 20150766.
34. Hu Y, Pan S, Zhao X, Guo W, He M, Guo Q. Value and clinical application of orthopedic metal artifact reduction algorithm in CT scans after orthopedic metal implantation. *Korean J Radiol* 2017; **18**: 526–35.
35. Oda S, Weissman G, Vembar M, Weigold WG. Iterative model reconstruction: improved image quality of low-tube-voltage prospective ECG-gated coronary CT angiography images at 256-slice CT. *Eur J Radiol* 2014; **83**: 1408–15.
36. Wellenberg RHH, van Osch JAC, Boelhouwers HJ, et al. CT radiation dose reduction in patients with total hip arthroplasties using model-based iterative reconstruction and orthopaedic metal artefact reduction. *Skeletal Radiol* 2019; **48**: 1775–85.
37. Neuhaus V, Grosse Hokamp N, Abdullayev N, et al. Metal artifact reduction by dual-layer computed tomography using virtual monoenergetic images. *Eur J Radiol* 2017; **93**: 143–8.
38. Zhang K, Han Q, Xu X, et al. Metal artifact reduction of orthopedics metal artifact reduction algorithm in total hip and knee arthroplasty. *Medicine* 2020; **99**: e19268.
39. Hwang JH, Kang JM, Park S, et al. Advanced virtual monoenergetic imaging algorithm for lower extremity computed tomography angiography: effects on image quality, artifacts, and peripheral arterial disease evaluation. *Diagn Interv Radiol* 2023; **29**: 175–82.
40. Matsuoka S, Hunsaker AR, Gill RR, et al. Vascular enhancement and image quality of MDCT pulmonary angiography in 400 cases: comparison of standard and low kilovoltage settings. *AJR Am J Roentgenol* 2009; **192**: 1651–6.
41. Zhao J, Cheng Q, Liu C, et al. Optimal combination periprosthetic vasculature visualization and metal artifact reduction by spectral computed tomography using virtual monoenergetic images in total hip arthroplasty. *Insights Imaging* 2023; **14**: 181.
42. Woo H, Chai JW, Choi YH, Jin KN. Metal Artifact Reduction for Orthopedic Prosthesis in Lower Extremity CT Venography: Evaluation of Image Quality and Vessel Conspicuity. *Cardiovasc Intervent Radiol* 2019; **42**: 1619–26.

Supporting Information

Additional supporting information may be found online in the Supporting Information section at the end of the article.

Table S1. The data obtained from regions R1 to R5 in computed tomography (CT) images without hip prostheses, the reference values of noise, mean Hounsfield unit (HU) and signal-to-noise ratio (SNR) at 80–140 kVp settings and reconstructed using filtered back projection (FBP), iDose^4 and IMR.

Table S2. The corrections made to the Hounsfield unit (HU) values, noise values and signal-to-noise ratio (SNRs) of region R1 (vascular region) using the O-MAR algorithm utilising FBP, iDose^4 and IMR for different kVp settings.

Table S3. The corrections made to the noise values, HU values and SNRs of region R5 using the O-MAR algorithm utilising FBP, iDose4 and IMR for different kVp settings.